A DNA Transformer for Visualizing Endogenous RNA Dynamics in Live Cells

Ying Wan,[†,‡] Ninghao Zhu,[†] Yi Lu,[†] Pak Kin Wong*[,†,§]

[†]Department of Biomedical Engineering, The Pennsylvania State University, University Park, PA 16802 USA.

[‡]School of Mechanical Engineering, Nanjing University of Science and Technology, Nanjing 210094, P. R. China.

[§]Department of Mechanical Engineering and Department of Surgery, The Pennsylvania State University, University Park, PA 16802 USA.

ABSTRACT: The functions of RNA are tightly regulated via diverse intracellular mechanisms. However, probing the complex dynamics of endogenous RNA in live cells is a challenging task. In the present study, a DNA transformer is designed for visualizing the abundance, distribution, and mobility of endogenous mRNAs in live human cells. The transformable tetrahedral DNA (T-TED) probe has a flexible hinge structure and is programmed to conform into a 3D tetrahedron upon binding with the target mRNA. By incorporating FRET imaging, super-resolution localization, and single particle tracking, the T-TED biosensor is applied for investigating the dynamics of Dll4 mRNA, which encodes a transmembrane protein, in human pulmonary microvascular endothelial cells. The data reveal unprecedented subpopulations of Dll4 mRNA with distinct mobility organized spatially in association with the endoplasmic reticulum and microtubule networks. The ability to monitor the dynamics of endogenous RNA in live human cells will provide a useful tool for studying the functions and regulation of RNA.

Recent studies have revealed functional complexity and diverse regulation mechanisms of RNA in mammalian cells.[1-4] In addition to the abundance, their subcellular localization and dynamic interaction with other intracellular components represent working strategies in the multifaceted modulation of RNA functions. For instance, β-actin mRNA is transported actively in the microtubule network to the lamellipodia during cell migration.[5] For mRNAs that encode transmembrane and secretory proteins, the signal recognition particle binds to the signaling sequence of the nascent polypeptide in the ribosome–mRNA-nascent polypeptide chain complex at the initiation of the translation process.[6, 7] The complexes are dynamically recruited to the endoplasmic reticulum (ER) and the secretory and transmembrane proteins are translocated into or across the ER membrane. The ER associated translational system has shown to be highly dynamic and is able to adapt cellular stimuli rapidly.[8, 9] These findings underscore the diversity and complexity of RNA regulation in human cells.

Visualization of RNA dynamics in live cells is essential for elucidating the molecular underpinnings of RNA processing, regulation, and functions. Fluorescent protein tagging, such as MS2 and MBSV6, multiply-labeled tetravalent RNA imaging probes, and aptamer-initiated fluorescence complementation are powerful strategies for monitoring dynamic gene expression in live cells.[10-13] Nevertheless, these techniques can be limited by the transfection efficiency, available colors, and requirement of genetic modification to express engineered transcripts containing multiple tandem repeats of the binding sequence.[14, 15] Nanoengineering strategies, such as nanoflares, gold nanorods, and graphene nanobiosensors, have been applied for dynamic gene expression analysis in live cells and intact tissue explants.[16-22] However, these methods introduce foreign materials in cells, which may increase cytotoxicity for delicate cells and affect their physiological functions.

Recently, DNA nanotechnology, such as framework nucleic acids and DNA origami, has drawn extensive attention for biomedical applications.[23-30] The monodisperse structures and inherent biocompatibility of DNA nanostructures enable intracellular sensing without the inhomogeneity and toxicity of inorganic nanomaterials.[31, 32] These DNA nanostructures can be internalized into mammalian cells via endocytosis for intracellular probe delivery, eliminating the requirement of transfection or microinjection.[33] DNA nanostructures also exhibit enhanced resistance to enzymatic degradation, which facilitate intracellular sensing.[34] In this study, we design a transformable tetrahedral DNA (T-TED) for probing RNA dynamics in live cells. Unlike existing DNA nanostructures that are often static, the T-TED probe is transformed into a 3D DNA tetrahedron upon binding with a target RNA (Figure 1A). The molecular transformation reaction brings the donor-acceptor pair into close proximity for FRET detection (Figure 1B). We characterize the T-TED biosensor for mRNA detection in human pulmonary microvascular endothelial cells (HPMEC). Single particle tracking, single molecule FISH, and colocalization studies are performed to investigate the dynamic of Delta-like ligand 4 (Dll4) mRNA, which regulates tip cell formation during angiogenic sprouting. The dynamics of Dll4 mRNA, which encodes a transmembrane protein, is investigated under DAPT treatment to explore the regulation of ER-associated translation.

EXPERIMENTAL SECTION

Materials. DNA strands used in this study were synthesized by Integrated DNA Technologies (Coralville, Iowa, USA). The

sequences are listed in Supplementary Table S1. All siRNAs were purchased from Santa Cruz Biotechnology (Dallas, Texas, USA). DAPT was purchased from Sigma (Saint Lious, Missouri, USA). TRIzol Plus RNA purification kit and Power SYBR®Green RNA-to-Ct™ 1-Step kit were purchased from Life Technologies Corporation (Waltham, Massachusetts, USA). Live cell endoplasmic reticulum (ER) staining kit was from AAT Bioquest, Inc (Sunnyvale, California, USA). Reagents for microtubule and lysosome staining were from Biotium, Inc (Fremont, California, USA). Single-molecule FISH experiments were performed using commercially available probes (Stellaris® RNA FISH probes) with CAL Fluor® Red 610. Lipofectamine 3000 for siRNA transfection was purchased from Invitrogen (Waltham, Massachusetts, USA).

Self-assembly and characterization of the T-TED biosensor. The T-TED probe was self-assembled according to a published protocol with minor modifications (Supplementary Fig. S1A).[35] Briefly, four DNA strands (T1, T2, T3, T4) with equal concentration of 1 μM were mixed in TM buffer solution (10 mM Tris and 5 mM $MgCl_2$). The mixture was heated to 95 °C for 5 min and quickly cooled down to 4 °C in 30 s. To characterize the emission spectra, samples were prepared in TM buffer. Fluorescence spectra were measured in flat bottom, black 384 well plates with clear bottom (Corning 3655) using a FlexStation 3 microplate reader equipped with a programmed temperature controller (Molecular Device, USA). The T-TED probe was excited at 488 nm.

Cell culture. HPMEC were cultured in medium 199 (Corning cellgro, MT10060CV) supplemented with 10% Fetal Bovine Serum (FBS; Atlanta Biologicals), 2 mM L-Glutamine, 100 U/ml Penicillin and 100 μg/ml Streptomycinpurchased. MCF-7 cells were cultured in DMEM with L-Glutamine, 4.5 g/L Glucose and Sodium Pyruvate (Corning MT10013CV), supplemented with 10% Fetal Bovine Serum (Corning MT35010CV). All cells were maintained in a humidified incubator (Thermo Forma 310) at 37 °C and 5% CO_2. HPMEC were seeded in a 24-well cell culture plate 24 h before transfection. The T-TED probe was added to the cells with a 100 nM concentration and incubated overnight. Cells were washed with PBS buffer three times before imaging. To upregulate Dll4 expression, DAPT was added to the cells with a 40 μM concentration after probe transfection. Dll4 and control siRNA were transfected into the cells by Lipofectamine 3000 according to the manufacturer's instruction. After transfection, cells were incubated for 24 h and then probes were transfected and incubated for overnight before imaging. For co-staining, ER, microtubule, and lysosome were stained after probe transfection. The cells were washed three times with PBS before imaging.

qRT-PCR. RNA samples from HPMEC under different conditions were collected using TRIZOL PLUS PURIFICATION kit following the manufacturer's instruction. The concentration of the total RNA was quantified with a NanoDrop 2000c (Thermo Fisher Scientific, USA). 10 μg total RNA was used for qRT-PCR with a Power SYBR Green RNA-to-Ct 1 step kit. qRT-PCR was performed using the CFX Connect real-time PCR system (Bio-Rad, USA).

Single particle imaging. Single particle tracking was performed using a Leica TCS SP8 confocal laser scanning microscope with an enclosure system (OKOlab, Italy) for temperature, humidity, and gas control. T-TED probes and ER staining were excited with a 488 nm solid-state laser. Microtubule and lysosome staining were excited with a 638 nm solid-state laser. Fluorescence signal was collected using an NA = 0.9, 63× air objective.

Particle Tracking and Data Analysis. Tracking of fluorescent particles was performed with the ImageJ plugin 'TrackMate'. Particles (diameter > 0.8 μm, threshold >1) were tracked in 200 frames to obtain the trajectories (imaging at one frames per second for 4 min). Statistical analysis was performed using Origin software. One-way ANOVA Tukey's post hoc test was used for multiple comparisons. The statistical significance was symbolized by ns ($p > 0.05$), * ($p \leqslant 0.05$), ** (p value $\leqslant 0.01$), *** (p value $\leqslant 0.001$), or **** (p value $\leqslant 0.0001$).

Equilibrium Analysis. We applied a computational model to study the detection capability of the biosensor.[36] The sigmoidal response curve was derived by solving the model using the Curve Fitting Toolbox of MATLAB (MathWorks, R2017b), after fitting the experimental data. The R^2 of the curve fitting is 0.985, suggesting the equilibrium analysis is capable of capture the variability of experimental data.

RESULTS AND DISCUSSION

T-TED biosensor for RNA detection in live cells. To create a transformable DNA nanostructure, the T-TED biosensor consists of four strands of DNA that form two triangular structures with two free chains and one common side, which serves as a flexible hinge (Figure 1A and Supplementary Figure S1A). Without a target mRNA, the DNA nanostructure separates the donor-acceptor pair due to electrostatic and steric repulsion. In the presence of a target RNA, hybridization induces a conformational change of the T-TED probe, which transforms the 2D nanostructure into a 3D tetrahedron, to allow effective energy transfer of the donor-acceptor pair (6-FAM and TEX615). Dynamic single cell analysis is achieved by the reversible conformational change of the DNA nanostructure.

Fluorescence spectroscopy was performed to characterize the FRET spectra and the performance of the T-TED probe (Figure 1B and Supplementary Figure S1B). By optimizing the operating condition, the T-TED probe features a considerably low detection limit of 30 pM (estimated based on three times of the standard deviation above the background) and high selectivity for single-base mismatch detection (Figure 1C-D and Supplementary Figure S1C-D). The DNA nanostructure also enables endocytic delivery of the T-TED probe into live cells with a high efficiency for intracellular RNA sensing. To evaluate the DNA transformer design for intracellular sensing, several T-TED probes were designed and evaluated in human pulmonary microvascular endothelial cells (HPMEC) (Figure 1E and Supplementary Figure S2). The probes were stable in cells for 2-3 days (Supplementary Figure S3). Single molecule RNA FISH was performed to evaluate the specificity of the T-TED probe (Supplementary Figure S4). By incorporating FRET imaging, the abundance and distribution of the target mRNA can be measured semi-quantitatively (Figure 1E). Single particle tracking can also be performed to investigate the dynamics of endogenous RNA in live cells (Figure 1F and Supplementary Movie M1).

Measuring RNA abundance in live cells by T-TED probes. To evaluate the ability of the T-TED probe for measuring the abundance of RNA transcripts, pharmacological

treatment and siRNA were employed for modulating the level of Dll4 mRNA in HPMEC (Figure 2A). The normalized intensity of individual cells was measured to quantify the signal. Treating the cells with DAPT, a Notch inhibitor, significantly increased the Dll4 mRNA signal while Dll4 siRNA reduced the signal compared to control siRNA (Figure 2B). Similar results were also observed in MCF7 cells (Supplementary Figure S5). The levels of mRNA were studied quantitatively by qRT-PCR (Figure 2C). The results demonstrated that DAPT led to an 8-fold increase in Dll4 mRNA while Dll4 siRNA reduced the transcript to an undetectable level. Comparison of the results suggested a sigmoid response of the T-TED biosensor, which is a characteristic of homogenous probes (Supplementary Figure S6).[36] The equilibrium binding reaction should be considered when quantitative results are required.

Single particle tracking of RNA by T-TED probes. The T-TED probe allows visualization of RNA molecules in live cells. We measured the distribution and dynamics of Dll4 and β-actin mRNA in HPMEC. Dll4 mRNA often localized near the nucleus while β-actin mRNA dispersed widely in the cytoplasm (Figure 3A-B). The dynamics of Dll4 mRNA and β-actin mRNA molecules were tracked for five minutes (Supplementary Movies M2 and M3). Single particle tracking with super-resolution localization allows subdiffraction estimation of the trajectory and displacement of the mRNA (Figure 3C-D). Molecules and clusters with diverse mobility values (instantaneous velocity from 0 to over 1 μm/s) were observed (Supplementary Figure S7). Some large immobile aggregates, which represent the background noise of the biosensor, were observed in the experiment. Figures 3F-G illustrate tracking of a Dll4 mRNA with super-resolution localization in a HPMEC cell. These values are in good agreement with other single particle trafficking studies.[37]

Mean square displacements (MSD) of Dll4 and β-actin mRNA were analyzed to evaluate the dynamics of the molecules (Figure 3E). For both β-actin and Dll4 mRNA, the MSD was approaching a plateau, suggesting corralled or confined diffusion of the transcripts. The MSD of corralled diffusion was modeled by the following Equation.[38]

$$\mathrm{MSD} = r_c{}^2\left[1 - \exp\left(-\frac{4\mathrm{Dt}}{r_c{}^2}\right)\right]$$

where r_c^2 is the plateau of the MSD curve and D is the diffusion coefficient. The diffusion coefficient of β-actin was estimated to be 0.1 $\mu m^2/s$, which is in excellent agreement with previous studies of β-actin mRNA using MS2.[5, 39] The diffusion coefficient of Dll4 mRNA was estimated to be 0.026 $\mu m^2/s$, which was significantly lower than β-actin mRNA. Dll4 mRNA also exhibited a lower plateau value compared to β-actin mRNA (7.74 μm^2 for Dll4 and 29.37 μm^2 for β-actin), suggesting Dll4 mRNA has distinct dynamics compared to β-actin mRNA.

DAPT treatment modulates the dynamics of Dll4 mRNA. We treated HPMEC with DAPT to investigate the regulation of Dll4 mRNA (Supplementary Movies M4 and M5). DAPT, a γ-secretase inhibitor, attenuates Notch signaling by preventing proteolytic cleavage of the Notch intracellular domain and enhances Dll4 expression.[40] In our experiment, DAPT treatment enhanced the MSD of the Dll4 mRNA in a time dependent manner (Figure 4A). Analyzing the MSD revealed that DAPT treatment did not have a significant effect on the diffusion coefficient (approximately 0.025 ± 0.01 $\mu m^2/s$ for all cases). Nevertheless, the plateau value increased from 7.74 μm^2 to 9.65 μm^2 and 11.03 μm^2 after 4 h and 20 h of DAPT treatment. To interrogate the increase in MSD, we analyzed the mobility of Dll4 mRNA. In this study, Dll4 mRNA molecules with instantaneous displacement values above 0.3 μm were defined as "mobile". This value is defined based on the resolution of our imaging system. Without DAPT treatment, approximately 58% of Dll4 mRNA were considered mobile in untreated cells. The value increased to 68% and 70% after 4 h and 20 h of DAPT treatment (Figure 4B). In contrast, examination of the mobile molecules revealed similar displacement with and without DAPT treatment (Supplementary Figure S8). These results demonstrate the ability of the T-TED biosensor for measuring the spatiotemporal dynamics of mRNA molecules and suggest that DAPT enhances the MSD of Dll4 mRNA primarily by increasing the percentage of mobile Dll4 mRNA, instead of modulating the dynamics of individual RNA.

Probing spatial organization of Dll4 mRNA dynamics. Our results indicated that DAPT increased the mobile subpopulation of Dll4 mRNA. We evaluated the spatial distribution and localization of these mobile transcripts. Interestingly, subpopulations with different mobility values exhibited distinct spatial distributions. Examining the distributions of immobile ($x < 0.3$ μm), intermediate (1.4 μm $> x > 0.3$ μm) and mobile ($x > 1.4$ μm) mRNA suggested DAPT modulated the spatial distributions of the mobile Dll4 mRNA (Figure 4C-D). In particular, a mobile subpopulation was induced in regions far away from the nuclei. Single particle tracking and velocity heat maps of Dll4 mRNA support this observation (Figure 4E-F and Supplementary Figure S9). Dll4 mRNA molecules near the nucleus tended to have a low mobility while a large portion of molecules far away from the nucleus exhibited a high mobility (Supplementary Figure S10).

Live cell staining of ER, microtubules, and lysosomes along with the T-TED probe was performed to investigate distribution and colocalization of the mobile subpopulation with other intracellular components (Figure 5A). ER staining illustrated that a high density of ER was located near the nucleus in HPMEC. Under control condition, the majority of Dll4 transcripts colocalized with the ER near the nucleus (Figure 5A). Approximately 86±8% (n=4) of Dll4 mRNA were associated with the high density ER near the nuclei. With DAPT treatment, Dll4 mRNA was upregulated and dispersed in the cytoplasm covering regions with both high and low density of ER (Figure 5B). The majority of mobile Dll4 mRNA induced by DAPT was located in the region with a low density of ER. These observations are consistent with the function of ER, which is responsible for translating secretory and transmembrane proteins. Colocalization further suggested that the mobile subpopulation was associated with the microtubule network. Figure 5C illustrates tracking of a Dll4 mRNA on microtubules. This observation suggests that the mobile Dll4 mRNA was actively transported via a microtubule-associated transport mechanism (Supplementary Movie M6).

This study reports the T-TED biosensor, a DNA transformer design, for probing the dynamics of endogenous RNA in live cells. The T-TED biosensor possesses several advantages and disadvantages compared to existing RNA sensing techniques.[41-43] First, the DNA nanostructure can be internalized into

mammalian cells with a high efficiency for detecting endogenous RNA. This characteristic avoids the issues associated with microinjection, transfection of plasmids and overexpression of exogenous reporters.[5] Second, the resistance of the DNA nanostructure allows single particle tracking and dynamic gene expression analysis for 2-3 days.[33] Third, the T-TED biosensor does not require metallic nanoparticles or other foreign materials[16-22] and is compatible with multiple human cell types. These advantages will facilitate the investigation of RNA dynamics in their native microenvironments. Nevertheless, the T-TED biosensor can have a lower signal-to-noise ratio compared to other approaches as only a single pair of fluorophores are employed. Non-specific binding, aggregation, and degradation of the probes can all contribute to the background signal of the T-TED biosensor. As shown in the single molecule FISH experiment, some spots observed may represent false positive signal, contributing to the background noise.

Using the T-TED biosensor along with single particle tracking, we investigated the dynamics of Dll4 mRNA, a transmembrane protein transcript, under DAPT treatment. The T-TED probe characterized the time-dependent upregulation of Dll4 mRNA by DAPT treatment. Interestingly, dynamic tracking identified a subpopulation of mobile Dll4 mRNA induced by DAPT. These mobile molecules have a similar diffusion coefficient before DAPT treatment, suggesting DAPT treatment did not modulate the ribosome–mRNA complex. In contrast, Dll4 increased the percentage of mobile Dll4 mRNA. Since the time scale (20 hours) is significantly longer than the upregulation of Dll4, the mobile subpopulation cannot be fully explained by the transient expression of Dll4. On the other hand, these unexpected mobile transcripts are spatially coordinated via the microtubule associated transportation mechanism in the region with a low density of ER. Classical studies suggested ER-bound ribosomes translate secretory and integral membrane proteins while free ribosomes contribute to cytosolic protein synthesis. The observation of the mobile Dll4 subpopulation in the low-density ER region, therefore, suggest another level of regulation may be involved in the translational dynamics of the ER associated translation system. Further investigation will be required to clarify the molecular origin and functions of the mobile Dll4 subpopulation.

CONCLUSIONS

In summary, we demonstrate a DNA transformer design for intracellular RNA sensing. Since the abundance, localization, and dynamic interactions with other intracellular components are fundamental strategies in RNA regulation, the T-TED biosensor possesses the potential to serve as a platform for investigating complex RNA dynamics in live cells.

ASSOCIATED CONTENT

Supporting Information.
The supporting information is available free of charge via the Internet at http://pubs.acs.org.

AUTHOR INFORMATION

Corresponding Author

*pak@engr.psu.edu

Notes

The authors declare no competing financial interest.

ACKNOWLEDGMENT

This work is partially supported by the NSF Biophotonic program and the Grace Woodward Grant from the Pennsylvania State University. The authors thank Peter Torab and William Hancock for technical discussion and critical review of the manuscript.

REFERENCES

(1) Dethoff, E. A.; Chugh, J.; Mustoe, A. M.; Al-Hashimi, H. M. *Nature* **2012**, *482*,322–330.
(2) Morris, K. V.; Mattick, J. S. *Nature Rev. Genet*. **2014**, *15*, 423–437.
(3) Wang, T. H.; Hamilla, S.; Cam, M.; Aranda-Espinoza, H.; Mili, S. *Nature Commun.* **2017**, *8*, 896.
(4) Buxbaum, A. R.; Haimovich, G.; Singer, R. H. *Nature Rev. Mol. Cell Bio.* **2015**, *16*, 95–109.
(5) Park, H. Y.; Lim, H.; Yoon, Y. J.; Follenzi, A.; Nwokafor, C.; Lopez-Jones, M.; Meng, X.; Singer, R. H. *Science* **2014**, *343*, 422–424.
(6) Palade, G. *Science* **1975**, *189*, 347–358.
(7) Walter, P.; Blobel, G. *J. Cell Biol.* **1981**, *91*, 551–556.
(8) Reid, D. W.; Nicchitta, C. V. *Nature Rev. Mol. Cell. Bio.* **2015**, *16*, 221–231.
(9) Reid, D. W.; Chen, Q.; Tay, A. S.; Shenolikar, S.; Nicchitta, C.V. *Cell* **2014**,.*158*, 1362–1374.
(10) Lionnet, T.; Czaplinski, K.; Darzacq, X.; Shav-Tal, Y.; Wells, A. L.; Chao, J. A.; Park, H. Y.; De Turris, V.; Lopez-Jones, M.; Singer, R. H. *Nature Methods* **2011**, *8*, 165–170.
(11) Tutucci, E.; Vera, M.; Biswas, J.; Garcia, J.; Parker, R.; Singer, R. H. *Nature Methods* **2017**, *15*, 81–89.
(12) Santangelo, P. J.; Lifland, A. W.; Curt, P.; Sasaki, Y.; Bassell, G. J.; Lindquist, M. E.; Crowe Jr, J. E. *Nature methods*, **2009**. *6*, 347–349.
(13) Valencia-Burton, M.; McCullough, R. M.; Cantor, C. R.; Broude, N. E. *Nature Methods* **2007**, *4*, 421–427.
(14) Hocine, S.; Raymond, P.; Zenklusen, D.; Chao, J. A.; Singer, R. H. *Nature Methods* **2013**, *10*, 119–121
(15) Weil, T. T.; Parton, R. M.; Davis, I. *Trends Cell Biol.* **2010**, *20*, 380–390.
(16) Briley, W. E.; Bondy, M. H.; Randeria, P. S.; Dupper, T. J.; Mirkin, C.A. *Proc. Natl. Acad. Sci. USA* **2015**, *112*, 9591–9595.
(17) Halo, T. L.; McMahon, K. M.; Angeloni, N. L.; Xu, Y.; Wang, W.; Chinen, A. B.; Malin, D.; Strekalova, E.; Cryns, V. L.; Cheng, C.; Mirkin, C. A. *Proc. Natl. Acad. Sci. USA* **2014**, *111*, 17104–17109.
(18) Wang, S.; Sun, J.; Zhang, D. D.; Wong, P. K. *Nanoscale* **2016**, *8*, 16894–16901.
(19) Wang, S.; Riahi, R.; Li, N.; Zhang, D. D.; Wong, P. K. *Adv. Mater.* **2015**, *27*, 6034–6038.
(20) Riahi, R.; Wang, S.; Long, M.; Li, N.; Chiou, P. Y.; Zhang, D. D.; Wong, P. K. *ACS Nano* **2014**, *8*, 3597–3605.
(21) Liu, Z.; Chen, S.; Liu, B.; Wu, J.; Zhou, Y.; He, L.; Ding, J.; Liu, J. *Anal. Chem.* **2014**, *86*, 12229–12235.
(22) Zhu, X.; Liu, Y.; Li, P.; Nie, Z.; Li, J. *Analyst* **2016**, *141*, 4541–4553.
(23) Lanier, L. A.; Bermudez, H. *Curr. Opin. Chem. Eng.* **2015**, *7*, 93–100.
(24) Li, J.; Pei, H.; Zhu, B.; Liang, L.; Wei, M.; He, Y.; Chen, N.; Li, D.; Huang, Q.; Fan, C. *ACS Nano* **2011**, *5*, 8783-8789.
(25) Tay, C. Y.; Yuan, L.; Leong, D. T. *ACS Nano* **2015**, *9*, 5609–5617.
(26) Xie, N.; Huang, J.; Yang, X.; Yang, Y.; Quan, K.; Wang, H.; Ying, L.; Ou, M.; Wang, K. *Chem. Commun.* **2016**, *52*, 2346–2349.
(27) Xie, N.; Huang, J.; Yang, X.; Yang, Y.; Quan, K.; Ou, M.; Fang, H.; Wang, K. *ACS Sensors* **2016**, *1*, 1445–1452.
(28) He, L.; Lu, D.; Liang, H.; Xie, S.; Zhang, X.; Liu, Q.; Yuan, Q.; Tan, W. *J. Am. Chem. Soc.* **2017**, *140*, 258–263.
(29) He, L.; Lu, D. Q.; Liang, H.; Xie, S.; Luo, C.; Hu, M.; Xu, L.; Zhang, X.; Tan, W. *ACS Nano*, **2017**, *11*, 4060–4066.

(30) Zhou, W.; Li, D.; Xiong, C.; Yuan, R.; Xiang, Y. *ACS Appl. Mater. Interfaces* **2016**, *8*, 13303–13308.
(31) Seabra, A. B.; Paula, A. J.; de Lima, R.; Alves, O. L.; Duran, N. *Chem. Res. Toxicol.* **2014**, *27*, 159–168.
(32) Bahadar, H.; Maqbool, F.; Niaz, K.; Abdollahi, M. *Iran. Biomed. J.* **2016**, *20*, 1–11.
(33) Liang, L.; Li, J.; Li, Q.; Huang, Q.; Shi, J.; Yan, H.; Fan, C. *Angew. Chem. Int. Ed. Engl.* **2014**, *53*, 7745–7750.
(34) Keum, J. W.; Bermudez, H. *Chem. Commun.* **2009**, *7*, 7036–7038.
(35) Pei, H.; Lu, N.; Wen, Y.; Song, S.; Liu, Y.; Yan, H.; Fan, C. *Adv. Mater.* **2010**, *22*, 4754–4758.
(36) Bonnet, G.; Tyagi, S.; Libchaber, A.; Kramer, F. R. *Proc. Natl. Acad. Sci. USA* **1999**, *96*, 6171–6176.
(37) Lifland, A. W.; Zurla, C.; Yu, J.; Santangelo, P. J.; *Traffic* **2011**, *12*, 1000–1011.
(38) Weigel, A. V.; Simon, B.; Tamkun, M. M.; Krapf, D. *Proc. Natl. Acad. Sci. USA* **2011**, *108*, 6438–6443.
(39) Fusco, D.; Accornero, N.; Lavoie, B.; Shenoy, S. M.; Blanchard, J. M.; Singer, R. H.; Bertrand, E. *Curr. Biol.* **2003**, *13*, 161–167.
(40) Shih, I. M.; Wang, T. L. *Cancer Res.* **2007**, *67*, 1879–1882.
(41) Vargas, D. Y.; Raj, A.; Marras, S. A.; Kramer, F. R.; Tyagi, S., Proc Natl Acad Sci U S A 2005, 102 (47), 17008-13.
(42) Shav-Tal, Y.; Darzacq, X.; Shenoy, S. M.; Fusco, D.; Janicki, S. M.; Spector, D. L.; Singer, R. H., Science 2004, 304 (5678), 1797-800.
(43) Turner-Bridger, B.; Jakobs, M.; Muresan, L.; Wong, H. H.-W.; Franze, K.; Harris, W. A.; Holt, C. E. Proceedings of the National Academy of Sciences 2018, 115, E9697-E9706.

TOC Graphic

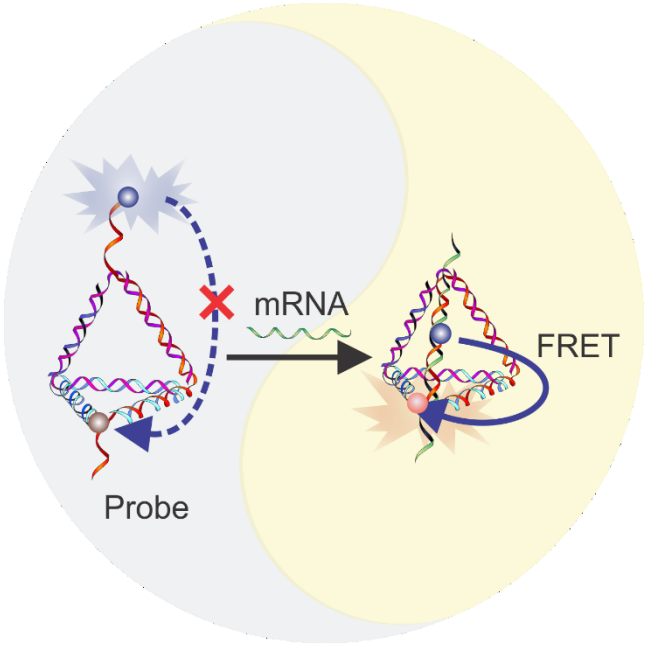

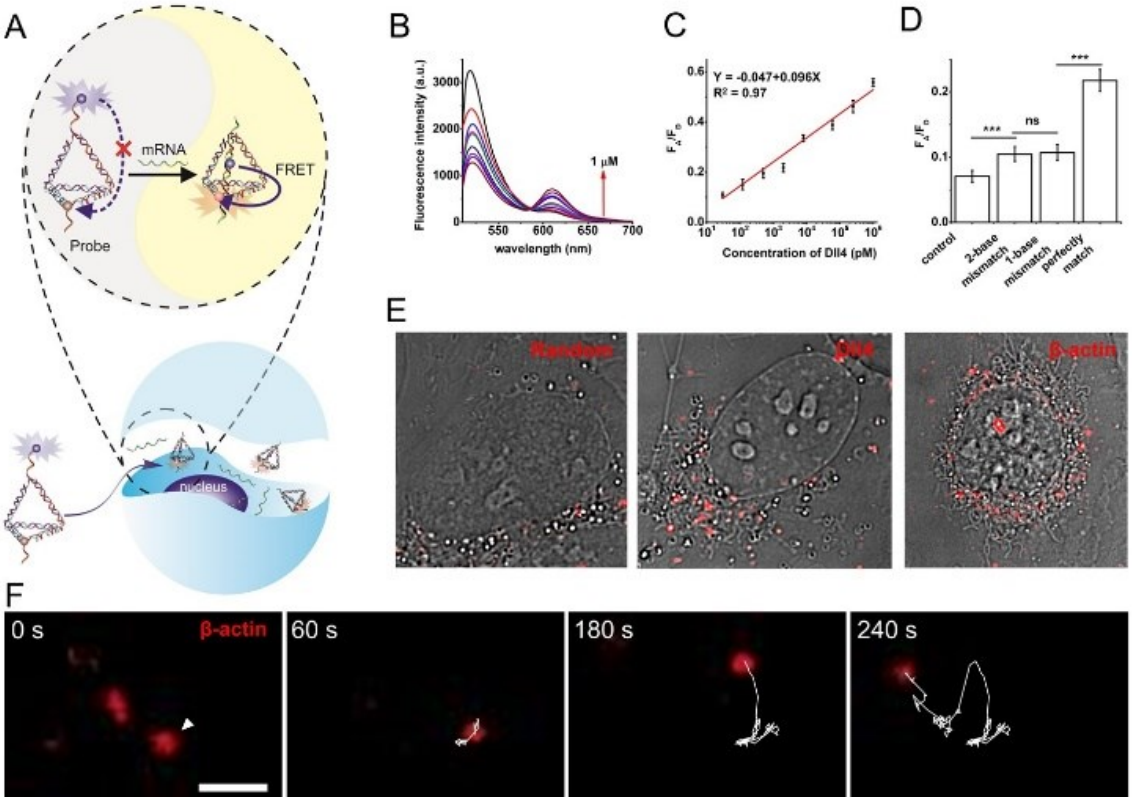

Figure 1. A transformable tetrahedral DNA (T-TED) biosensor for visualizing RNA dynamics in live cells. (A) Schematic illustration of the detection strategy of the T-TED biosensor. (B) FRET spectra of the T-TED probe for detecting target sequences at different concentration. (C) Calibration curve of T-TED biosensor (F_A/F_D represents the intensity ratio between the acceptor and the donor). (D) Selectivity of the probe for 1-base and 2-base mismatch detection at 1 nM target concentration. (n=3, one-way ANOVA followed by Tukey's post hoc test, ***, $p<0.001$). (E) Confocal images of random, Dll4 and β-actin probes for intracellular detection in HPMEC. Images are representative of at least five experiments. Scale bars, 20 μm. (F) Single particle tracking of β-actin mRNA in a HPMEC cell for 240 s. White line shows the trajectory of the mRNA determined by super-resolution localization. Scale bar, 2 μm.

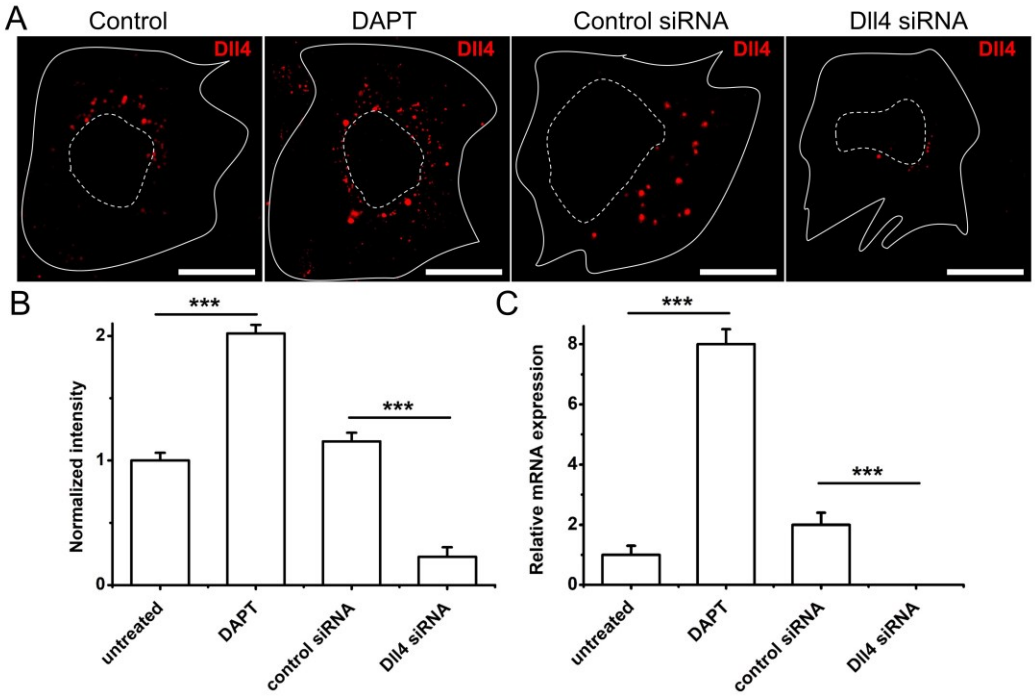

Figure 2. Quantification of Dll4 mRNA in live cells. (A) Confocal images illustrating Dll4 mRNA detection in HPMEC with control, DAPT, control siRNA, and Dll4 siRNA. Solid lines indicate the cell boundaries and dash lines indicate the cell nuclei. Images are representative of five experiments. Scale bars, 20 μm. (B) Normalized intensity for Dll4 mRNA detection with the T-TED biosensor ($n \geqslant 9$, one-way ANOVA followed by Tukey's post hoc test, ***, $p < 0.001$). (C) Relative Dll4 mRNA expression level in HPMEC detected by qRT-PCR ($n = 3$, one-way ANOVA followed by Tukey's post hoc test, ***, $p < 0.001$).

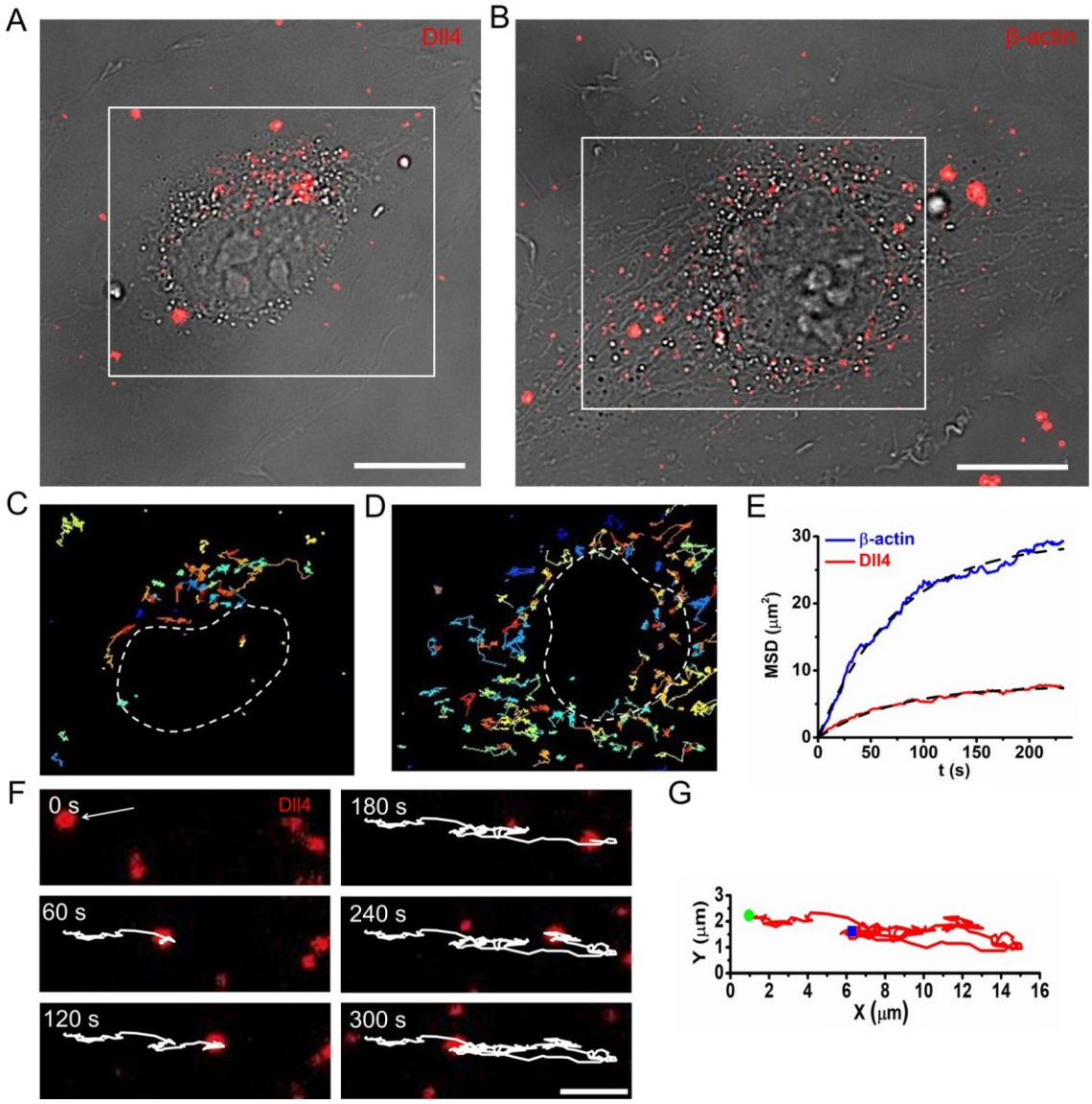

Figure 3. Single particle tracking by the T-TED biosensor in live cells. (A-B) Images of Dll4 and β-actin mRNA distributions in HPMEC. White rectangles indicate regions for single particle tracking in C and D. Scale bars, 20 μm. (C-D) Trajectories of Dll4 and β-actin mRNA in selected regions in A and B. Each color line represents the trajectory of a single particle. Dash lines indicate the nuclei of the cells. Data are representative of five independent experiments. (E) Mean squared displacement (MSD) of Dll4 and β-actin mRNA in HPMEC (Dll4, n = 153; β-actin, n = 119). Dash lines indicate corralled diffusion fitting curves. (F) Single particle tracking of a Dll4 mRNA in a HPMEC for five minutes. White lines show the trajectories of the mRNA determined by super-resolution localization. Scale bar, 2 μm. (G) The trajectory of the Dll4 mRNA in F. Green dot represents the initial position and blue dot represents the final position.

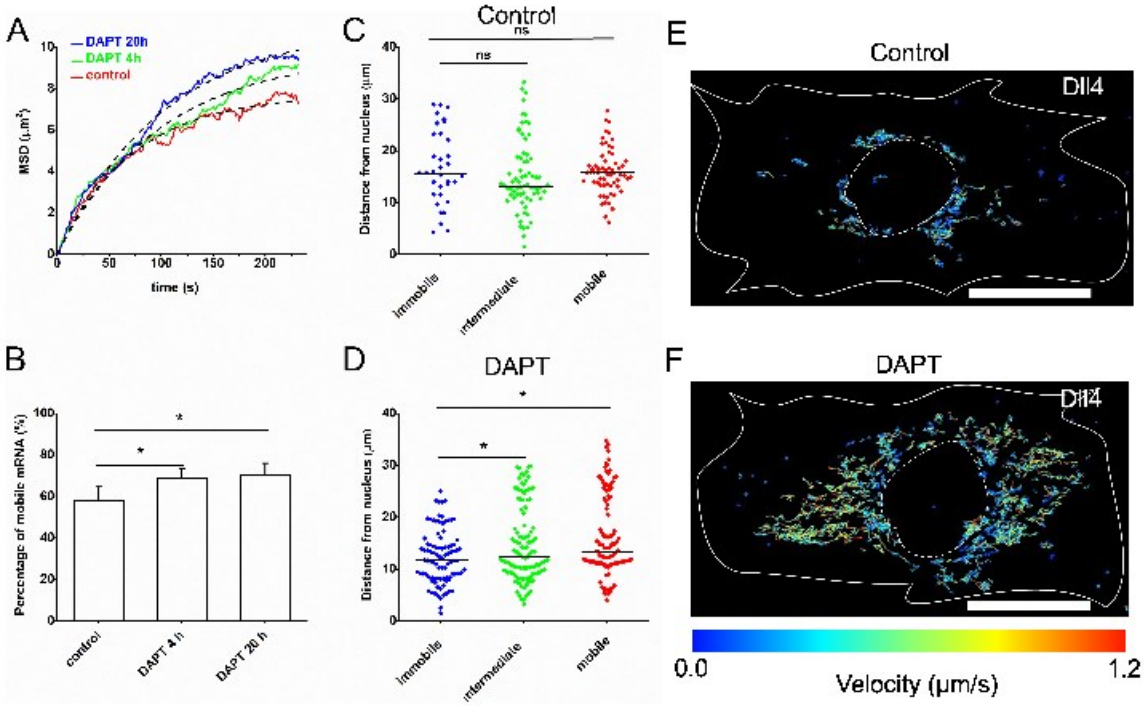

Figure 4. Dynamics of Dll4 mRNA with DAPT treatment. (A) MSD of Dll4 mRNA in HPMEC before and after DAPT treatment (n ≥ 153). (B) Percentage of mobile Dll4 mRNA before and after DAPT treatment (n≥5, one-way ANOVA followed by Tukey's post hoc test, *, $p < 0.05$). (C) Spatial distributions of Dll4 mRNA in control. Based on the maximum displacement, Dll4 mRNA molecules were classified into immobile ($x < 0.3$ μm), intermediate (1.4 μm $> x > 0.3$ μm) and mobile ($x > 1.4$ μm). (D) Spatial distributions of Dll4 mRNA with DAPT treatment (n ≥ 93, one-way ANOVA followed by Tukey's post hoc test, *, $p < 0.05$, ns, not significant). (E-F) Velocity heat maps of Dll4 mRNA in (E) control cells and (F) DAPT treated cells. Color lines represent traces of individual Dll4 mRNA. Color bar represents the instantaneous velocity of the molecule in the trace. Images are representative of five experiments. Solid lines indicate the cell boundaries and dash lines indicate the cell nuclei. Scale bars, 20 μm.

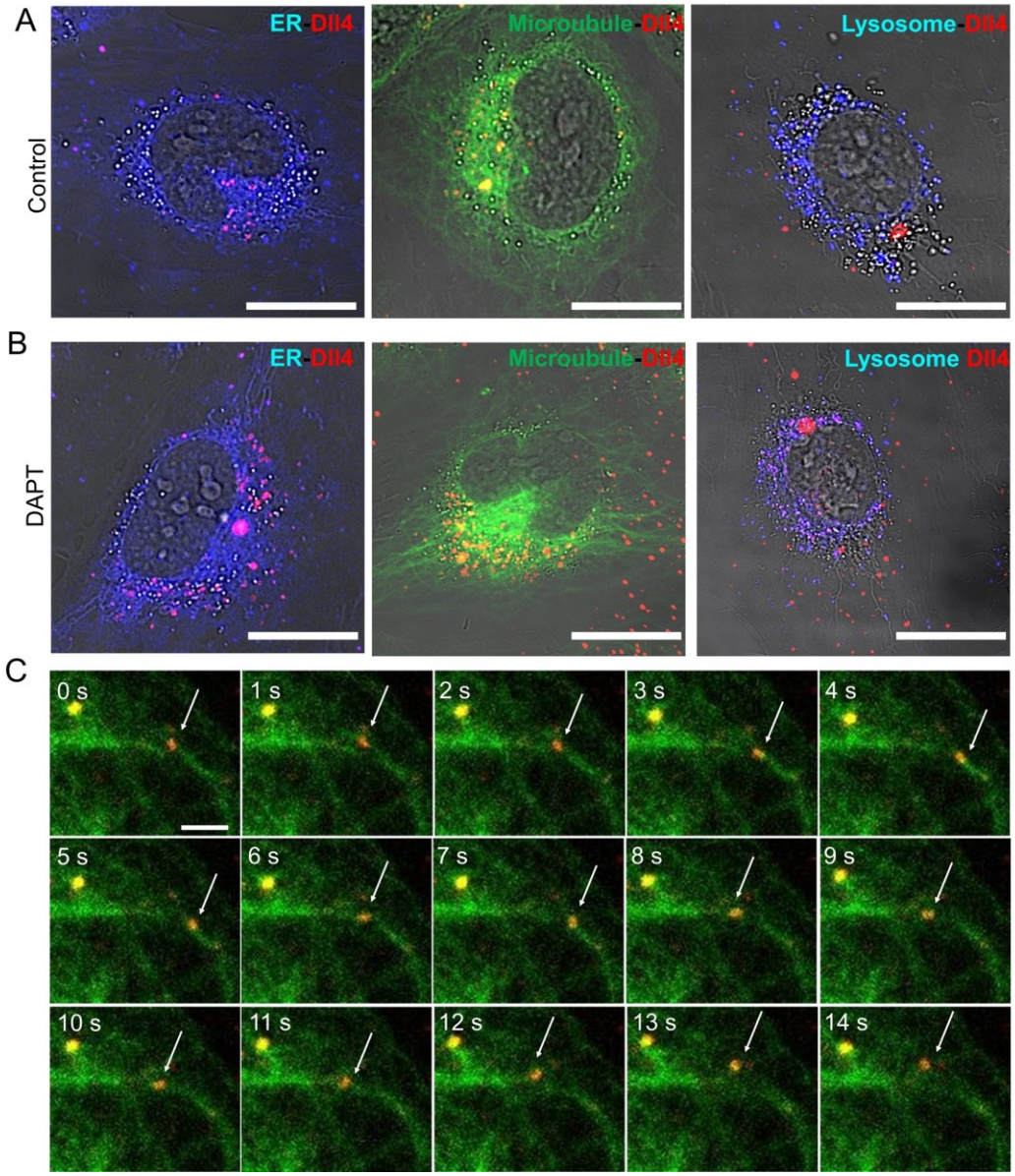

Figure 5. Colocalization of Dll4 mRNA with other intracellular components. (A-B) Colocalization of Dll4 mRNA with ER, microtubule, and lysosome in (A) control cells and (B) DAPT treated cells. Images are representative of five experiments. Scale bars, 20 μm. (C) Time-lapse images of a Dll4 mRNA (white arrows) trafficking on microtubules. Scale bar, 2 μm.